



Deposited via The University of Sheffield.

White Rose Research Online URL for this paper:

<https://eprints.whiterose.ac.uk/id/eprint/176037/>

Version: Accepted Version

Article:

Leventea, E., Zhu, Z., Fang, X. et al. (2021) Ciliopathy genes are required for apical secretion of Cochlin, an otolith crystallization factor. *Proceedings of the National Academy of Sciences*, 118 (28). e2102562118. ISSN: 0027-8424

<https://doi.org/10.1073/pnas.2102562118>

© 2021 The Author(s). This is an author-produced version of a paper subsequently published in *Proceedings of the National Academy of Sciences*. Uploaded in accordance with the publisher's self-archiving policy.

Reuse

Items deposited in White Rose Research Online are protected by copyright, with all rights reserved unless indicated otherwise. They may be downloaded and/or printed for private study, or other acts as permitted by national copyright laws. The publisher or other rights holders may allow further reproduction and re-use of the full text version. This is indicated by the licence information on the White Rose Research Online record for the item.

Takedown

If you consider content in White Rose Research Online to be in breach of UK law, please notify us by emailing eprints@whiterose.ac.uk including the URL of the record and the reason for the withdrawal request.

Ciliopathy Genes are required for apical secretion of Cochlin, an otolith crystallization factor

Leventea, Eleni¹, Zhu, Zhou^{1*}, Fang, Xiaoming^{1*}, Nikolaeva, Yulia¹, Markham, Eleanor¹ Hirst, Robert A.², van Eeden, Fredericus J.M.^{1,3} & Malicki, Jarema J.¹

¹University of Sheffield, Department of Biomedical Science, Western Bank, Sheffield, S10 2TN, United Kingdom

²Department of Respiratory Sciences, College of Life Sciences Room 247, Maurice Shock Building, University of Leicester, University Road, Leicester, UK LE1 7RH

³Corresponding author.

*Equal contribution.

Abstract

Here we report that important regulators of cilia formation and ciliary compartment-directed protein transport function in secretion polarity. Mutations in cilia genes, *cep290* and *bbs2*, involved in human ciliopathies, affect apical secretion of a Cochlin, a major otolith component and a determinant of calcium carbonate crystallization form. We show that Cochlin, defective in human auditory and vestibular disorder, DFNA9, is secreted from small specialized regions of vestibular system epithelia. Cells of these regions secrete Cochlin both apically into the ear lumen and basally into the basal lamina. Basally secreted Cochlin diffuses along the basal surface of vestibular epithelia, while apically secreted Cochlin is incorporated into the otolith. Mutations in a subset of ciliopathy genes lead to defects in Cochlin apical secretion causing abnormal otolith crystallization and behavioral defects. This study reveals a class of ciliary proteins are important for the polarity of secretion and delineate a novel secretory pathway that regulates biomineralization.

Significance Statement

We found that genes associated with human ciliopathies modulate apico-basal polarity of secretion. In addition, we show that this is essential for Cochlin function, the protein associated with DFNA9, a human non-syndromic deafness with vestibular dysfunction. Cochlin is secreted by a group of specialized epithelial cells both apically and basally in the ear. We found that apically secreted Cochlin is essential for proper otolith formation. In this way, we offer a plausible molecular explanation why DFNA9 patients suffer from balance disorders. The involvement of cilia genes in polarized secretion is an entirely new function for this otherwise very well studied and medically important group of genes.

Introduction

Cilia are finger-like cell surface protrusions involved in an immense array of biological processes that range from limb patterning in the embryo to light detection in the eye. Numerous cilia genes are associated with human disorders collectively known as ciliopathies. While analyzing cilia function in vertebrate sensory organs, we focused on Cep290, a protein that localizes to centrosomes and the ciliary transition zone. Human *CEP290* defects range from blindness to severe developmental defects causing perinatal lethality (1, 2). Otoliths are highly mineralized

bodies that rest on the surface of sensory epithelia in the vestibular system of vertebrates. Otolith displacement that occurs in response to body movements stimulates mechanosensitive hair cells embedded in sensory epithelia, providing the organism with information about body position (3). The main inorganic component of the otolith is calcium carbonate (CaCO₃). Its crystal form (polymorph) varies across species and in different otolithic organs. Otolith calcium carbonate crystal form is controlled by proteinaceous matrix that remains poorly characterized, and which is thought to control the balance between calcite, vaterite and aragonite (4). In teleost fish, the utricular otolith mainly contains aragonite, the latter can be detected by Meigen's Cobalt Nitrate stain (5-7). Defects in certain otolith matrix proteins lead to the appearance of other calcium carbonate polymorphic forms and abnormal crystal morphology (6). In humans and animals, this is likely to affect vestibular function and result in behavioral defects (8, 9).

Materials and Methods

Zebrafish Strains and Maintenance

All animal studies were performed in accordance with the UK Home Office regulations and the UK Animals (Scientific Procedures) Act 1986. The *cep290*^{sa1383}, *bbs2*^{sa2952} and *bbs9*^{sa14425} alleles were obtained from the Sanger Institute TILLING project. The *ovl*^{tz288b} allele was previously used for cilia analysis by us (10). Cochlin mutants were generated using the CRISPR/ Cas9 system, with gRNAs targeting exons 11 and 12 (CCATGCCCAGTTGGTTCAGCACC for vWF1 and GGCGATGGCGTCTGAGCCCAAGG for vWF2). To generate *cochlin* crispants 4 guides were injected against exon 2 (CTTCATTAACCATGTCGTTG), exon 3 (CAGGTATTCTCTTTGAGC) and 2x exon 4 (GTTGCAACGCCGATTAGCTG, TATGCGGAGCAGCCATTCAC). Genotypes were determined by finclipping adult fish, followed by DNA isolation, PCR amplification of mutation sites and Sanger sequencing. Genotyping primers are provided below (Table 1). Phenotypic analysis was performed by comparing homozygous mutants and heterozygous or wild-type animals derived from the same ancestral line. For phenotypic analysis crosses were repeated at least twice. Heat-shock promoter driven *Ar113b-EGFP-Inp54*^{D281A} transgenic line was used to visualize cilia. To activate expression, transgenic animals were heat shocked at 4.5 dpf for 30 min. at 39°C and fixed 12 hours later. Expression was analyzed on cryosections as described for immunostaining below.

Table 1 Genotyping primers

| Gene | Forward | Reverse |
|--------------------------------|------------------------------------|--------------------------------|
| <i>cep290^{sa1383}</i> | CAAGGATCTTCAGAGGAGCC | CATGACCTTAACCATTACAGTAC |
| <i>bbs2^{sa2952}</i> | GGGAAACCTTATGGACTCAAGC | CATGTCTAACCTTGGCATTTCCTC |
| <i>bbs9^{sa1425}</i> | TTTCCATATGTATGGTTTTCTCA GGCACCG | CGATTACCTGTAACACCACCGAATG |
| <i>coch^{sh536}</i> | GTGTGAACCTCTGACTCTCC | CATCTGATCGATGGAGC |
| <i>coch^{sh555}</i> | GAATCACTGTTTACGCAGTGG | TGCACTCAAGAAAATCTCAAATTGT C |

Behavioral Analysis

For swimming behavior assay, 5 dpf larvae were placed in wells of a standard 24-well dish each filled with 1 mL of E3 medium and left to acclimatize for 30 minutes in the Zebrabox chamber (ViewPoint Behavior Technology). Stress response of larvae was tested by modifying a previous protocol (11): a drop of 4M NaCl was added to each well resulting in the final concentration of roughly 250mM NaCl. Following 10 minute incubation, the NaCl solution was replaced with fresh E3 medium for the remainder of the assay. Swimming behavior of larvae (total distance, duration of movement, inactive time, speed) was tracked for 10 minutes after E3 replacement using the Zebrolab software. High (magenta $>10\text{mms}^{-1}$), medium (green) and low speed (black $<3\text{mms}^{-1}$) were annotated. Approximately 12 heterozygous and 12 mutant larvae were tested in parallel in each experiment.

Adult zebrafish behavior was recorded using the Zebrabox tracking system and software as above. Adult zebrafish, approximately 3 months of age, were placed in beakers filled with 300 ml of aquarium water and were acclimatized for one hour in the Zebrabox chamber. Swimming activity was tracked for 10 minutes with constant light at 15% intensity inside the tracking chamber High (magenta $>6\text{cms}^{-1}$) medium (green) and slow speeds (black $<3\text{cms}^{-1}$) were annotated.

Ciliary motility recording

High resolution ciliary beat analysis was done using a Zeiss Axioscope attached to an IDT MotionPro X4 high-speed camera. Movies were recorded at 500fps (x1000 magnification) and

slow motion playback of captured sequences allowed the determination of ciliary beat frequency and beat pattern. CBF calculation was done by dividing the frame rate (500) by the number of frames elapsed for the observer to count 5 ciliary beat cycles, multiplied by 5 to convert to beats per second (Hz).

Otolith Crystal Polymorph Determination

Utricular otoliths were dissected and washed with deionized water for 5 min. as described (12). They were then boiled in 0.5M solution of cobalt nitrate (7) (102536, Merck Millipore) for 4 minutes and photographed immediately thereafter. 6 otoliths from 3 individuals were used for *coch* *bbs2* and *bbs9*, 20 otoliths were used for *cep290*.

Proteomic Analysis

Dissected utricular otoliths were decalcified overnight at 4°C in 0.2M EDTA in 100mM Tris pH 8.0. 4 otoliths from two fish were used for each experiment. After overnight incubation in EDTA, a transparent structure remained at the bottom of the tube, representing the decalcified protein matrix of the otoliths, which was homogenized using a hand-held homogenizer (47747-370, VWR). The samples were subsequently centrifuged on a benchtop centrifuge at 4°C for 30 minutes at 13,000 rpm. After centrifugation, a pellet becomes apparent at the bottom of the tube and the supernatant was transferred into a new tube and mixed with an equal volume of 2x Laemmli buffer. This provided the soluble fraction of otolith proteins. The pellet was washed with cold acetone and centrifuged at 4°C for 20 minutes at 13,000rpm. Acetone was removed and the pellet air dried for 15 minutes. 20ul of 2x Laemmli buffer was added to the tube and the pellet was homogenized with a pestle providing insoluble fraction. Both soluble and insoluble fractions were heated to 95°C for 10 min. and loaded on a 10% SDS-PAGE gel along with a Spectra Multicolor pre-stained protein ladder (26623, ThermoFisher Scientific). Electrophoresis was performed at 100V for 2 hours using the Mini-Protean Tetra system (Bio-Rad), after which gel was washed with dH₂O for 20 minutes on an orbital shaker at room temperature and fixed overnight in a 40% methanol, 10% acetic acid, 50% dH₂O solution. Fixation solution was replaced with Coomassie Brilliant Blue R staining solution (161-0436, Bio-Rad) and incubation continued on an orbital shaker for 4 hours at room temperature. To destain, gel was placed in dH₂O and microwaved 6 times, 1 minute each, followed by incubation for 30 minutes at 37°C. Gel was

photographed using a white light transilluminator. Individual bands were excised with a scalpel blade and Mass Spectrometry was performed at Harvard Medical School-Taplin Mass Spectrometry Facility.

Western Blotting

For western blot analysis, 2-3 otoliths were used to obtain insoluble fraction as above. Alternatively, adult fish head was homogenized using the same homogenizer as above in approximately 0.3 ml of lysis buffer (40mM PIPES, 100mM MgCl₂, 50mM EDTA, 400mM NaCl). For westerns of larvae ~100 larvae were homogenized using a pestle in RIPA buffer. The homogenate was diluted in equal volume of 2x Laemmli buffer and heated to 95°C for 5 min. Proteins were separated on 12% SDS-PAGE gel, transferred to nitrocellulose membrane (Amersham GE Healthcare) and stained with anti-Cochlin primary antibody (1:800-1000, Proteintech, custom made) and anti-rabbit IgG, HRP (1:10,000, Abcam, ab97051) secondary antibody. Membranes were incubated in Pierce ECL Western Blotting Substrate according to manufacturer's instructions. Staining was visualized using the ChemiDoc MP Imaging System (Bio-Rad).

Immunohistochemistry

Zebrafish larvae were cryosectioned and immunostained using standard protocols (12). For Cochlin, larvae were fixed in 4% PFA overnight at 4°C and treated using an antigen retrieval protocol (13) prior to sectioning and immunostaining. Dent's fixative overnight at 4°C was used for Cep290 staining. The following primary antibodies and dilutions were used: anti-acetylated tubulin (1:500-1000, Sigma, T6793); anti-Cochlin (1:1000, Proteintech, custom made). ZO-1 (mouse) 1A12, Invitrogen, Cat. 33-9100, dilution (1:200) PKC zeta /αPKC (rabbit poly), Santa Cruz Biotechnology, Cat. sc-216, dilution (1:50), Rab8a (Novus, clone 3G1, mouse monoclonal, 1:200), Rab11 (Cell Signaling, D4F5, rabbit mAb, 1:200). Prior to imaging, sections were counterstained with DAPI for 30 min. to visualize nuclei. Images were collected with an Olympus FV1200 confocal microscope equipped with a 40x, NA 1.0 or 60x, NA 1.42 oil lens. Red signals were converted to magenta using Photoshop.

Microscopy & Photography

To evaluate otolith shape, 1.5 dpf larvae were dechorionated, anesthetized in 0.168% wt/vol Tricaine (Sigma, E10521) in E3 media (14), positioned in 3% methylcellulose with the lateral side up and photographed using Zeiss Axio Zoom V16 microscope and PlanNeoFluar 1x/0.25 FWD 56mm lens. Alternatively, Zeiss Axio Observer inverted microscope and 20x NA 0.5 Plan NeoFluar lens was used.

Adult fish were photographed after being anesthetized in Tricaine diluted in aquarium water as above. Animals were positioned with the lateral side up in plastic boats (VWR) filled with 20 mL of Tricaine solution. Photographs were obtained using a 12 megapixel digital camera. For scanning electron microscopy of otoliths of adult individuals were dissected, washed in PBS for 10 minutes, fixed in 4% PFA overnight at 4°C and left in 1 ml of 100% ethanol for 24 h in an open glass dish to allow ethanol evaporation. Larvae were fixed in 2.5% glutaraldehyde in 100mM Na cacodylate buffer (pH7.5) overnight, washed in buffer, 1 hr post fixed in 2% OsO₄, washed again and dehydrated in an ethanol series before drying in a mixture of 50% Hexamethyldisilazane (HEX) in 100% ethanol and final drying in 100% HEX, after removal of this solution larvae were left to dry overnight in a fume hood. Dried larvae were broken using watch makers forceps under a stereomicroscope to expose the inner ear vesicle. If required, the otolith was removed. Adult otoliths or larvae were then immobilized on carbon adhesive discs mounted on SEM sample stubs, coated with gold using Edwards S150B Gold Sputter Coater and imaged on Phillips XL-20 or Tescan Vega3 microscope.

In situ hybridization

The *cochlin* probe was synthesized using zebrafish cDNA clone obtained by Dharmacon (EDR5649-213361471) using standard protocols (14). Hybridisation, washes, signal detection and postfixation were carried out as published (15). For photography, larvae were positioned in 3% methylcellulose and photographed using Axio Zoom V.16 Zeiss microscope with a PlanNeoFluar 2.3x/0.57 FWD 10.6mm lens. To study expression further, larvae were embedded in Epon using standard protocols (12) and sectioned at 10 µm on Reichert-Jung Ultracut E ultramicrotome. Sections were counterstained with DAPI and photographed using Zeiss Axio Observer inverted microscope and 100x, NA 1.4 oil lens.

Morpholino Knockdown

Morpholino knockdowns were performed as described previously (12, 16). Coch ATG: GGACAGCAAACCAACAACGACATGGT, Coch Sp: AAGTGAAAACCTGTACCTGTGAATGG
Control: CCTCTTACCTCAGTTACAATTTATA

Statistical Analysis

Statistical analysis was carried out using Student's *t* test, chi-squared test or Kruskal-Wallis test included in GraphPad Prism 7.0 software (<http://www.graphpad.com/>). Data are represented as mean \pm 95% confidence interval (95% CI). Significance is represented as follows: * for $p < 0.05$, ** for $p < 0.01$, *** for $p < 0.001$, **** for $p < 0.0001$.

Results

The zebrafish *cep290*^{sa1383} mutant allele does not cause obvious developmental defects (Fig. 1a), and confirmed by sequencing the correct mutation was present in the fish (Fig. 1b,c). We noticed, however, that mutant larvae that become hyperactive in response to osmotic shock (Fig. 1d, f). Similarly, adult homozygotes swam more actively, compared to wild-type controls (Fig. 1e, g). To investigate whether this behavior is due to vestibular abnormalities, we dissected otoliths and analyzed them using scanning electron microscopy (SEM). In contrast to wild-type utricular otoliths, which have smooth surface, mutant otoliths form sharp ridges (Fig. 2a). In the zebrafish embryo, 2 equally sized otoliths are developed on the second day of development (17, 18). Morphologically defective otoliths are also transiently present in *cep290*^{sa1383} embryos, where they are either strongly unequal in size or there are more than 2 otoliths present, often close together and perhaps in the process of fusion (Fig. 2b, c). Otolith defects could be the result of defects in cilia formation or function in the ear, however we were not able to detect such defects in *cep290*^{sa1383} larvae using various assays (Extended Data Fig.1, Movies S1, S2).

Otolith morphology defects that we observed in Cep290 mutants suggested that calcium carbonate does not crystallize properly in the mutant strain. To determine whether CaCO₃ crystal polymorph is affected by *cep290*^{sa1383} mutations, we stained otoliths with cobalt nitrate (7). Mutant otoliths display more intense brown staining (Fig. 2d), revealing increased aragonite content. This result shows that Cep290 functions in a process that regulates CaCO₃ crystallization.

Abnormal CaCO₃ crystallization suggested that secretion of otolith proteins by ear epithelia was affected in our *cep290^{sa1383}* allele. Electrophoretic analysis of protein content from wild-type and *cep290^{sa1383}* mutant otoliths revealed that, indeed, a prominent band of ca. 42kDa is significantly reduced in the mutant (Fig. 3a, arrow). Based on mass spectrometry, we determined that the missing protein is Cochlin (Extended Data Fig. 2). Cochlin contains two von Willebrand Factor (vWF) domains and an N-terminal LCCL domain, homologous to a hemolymph coagulation factor (Fig. 3b), known to be proteolytically removed in some tissues (19, 20). The vWF domains are found in complement proteins and extracellular matrix components, including collagens. Cochlin fragments are secreted into bloodstream during inflammation(19). Secretion into the ear lumen has not been, however, reported thus far, possibly due to different protein extraction methods used. The 42kDa band that we identified in the otolith corresponds to the processed form of Cochlin with the LCCL domain removed (Fig. 3a, Extended Data Fig. 3).

Human missense mutations in Cochlin are associated with autosomal dominant hearing loss (DFNA9)(19, 21). Consistent with otolithic defects, both human and mouse *cochlin* mutations result in vestibular malfunction (22, 23) which, in the mouse, precedes hearing loss (23). Human mutations also cause vertigo in some patients (22). In spite of this, Cochlin presence in otoliths has not been previously reported.

To investigate Cochlin function further, we generated deletion alleles in each VWF domain (Fig. 3b). Similar to *cep290^{sa1383}* mutants, *coch*^{-/-} mutant homozygotes and morphants display otolith defects at 36 hpf (Fig. 3c; Extended Data Fig. 4). *Coch* crispants also showed hyperactivity in response to osmotic shock (Extended Data Fig. 4e). Otoliths of adult *coch*^{-/-} homozygotes form sharp crystals and display grossly abnormal shape (Fig. 3d, Extended Data Fig. 5). Compared to *cep290^{sa1383}* mutants, these defects occur earlier and are more severe. Cobalt nitrate staining confirmed overabundance of aragonite in *coch*^{-/-} otoliths (Fig. 3e). These findings show that Cochlin functions as a CaCO₃ crystallization determinant.

Cep290 physically interacts with proteins encoded by Bardet-Biedl Syndrome (BBS) genes, thought to be involved in intracellular transport (24-26). To test whether BBS proteins also affect Cochlin secretion, we characterized *bbs2^{sa2952}* and *bbs9^{sa14425}* mutants (Fig.4a,d ; Extended Data

Fig.6). Both mutants display transient otolith defects at 36 hpf (Fig. 4b, e). *bbs2*^{+/-}; *cep290*^{sa1383/+} and *bbs9*^{+/-}; *cep290*^{sa1383/+} double heterozygous embryos also display otolith defects revealing genetic interaction between *cep290* and *bbs* loci (Fig.4c, f). SEM on otoliths from *bbs2*^{-/-} adult homozygotes revealed somewhat abnormal crystallization (Extended Data Fig. 6). Moreover, cobalt nitrate staining is more prominent in otoliths from these animals (Fig. 4g). By contrast, otoliths from *bbs9*^{-/-} homozygotes display largely normal cobalt staining (Fig. 4g). These data show that Cep290 and its interaction partners first function transiently during embryogenesis in otolith formation and later in life facilitate Cochlin secretion and otolithic calcium carbonate crystallization.

To determine which cells secrete Cochlin, we first performed in situ hybridization on embryos and larvae. *Cochlin* transcript is expressed at a high level in the ear (Extended Data Fig. 7). On sections, high expression is visible at the anterior and medial edge of the utricular macula and at the dorsal and to a lesser extent ventral edge of the saccular macula (Fig. 5a, Extended Data Fig.7). To localize Cochlin polypeptide, we performed antibody staining on sections through the ear. This analysis revealed high level of Cochlin in small groups of cells immediately adjacent to sensory maculae but not in hair cells (Fig. 5b-d, Extended Data Fig. 1, 8). Consistent with its secretion and incorporation into the otolith, Cochlin signal accumulates in the apical cytoplasm of these cells (Fig. 5d, arrows). Cochlin is also abundantly present in the basal lamina of epithelia lining ear cavity (Fig. 5b, c, arrowheads). Compared to *cochlin* transcript, Cochlin protein is found over much larger area, indicating that it diffuses long distances along the basal surface of epithelia, or that cochlin expression may be more widespread at earlier stages.

While secretory vesicles of Cochlin accumulate apically in cells adjacent to sensory maculae of the wild-type ear, in *cep290*^{sa1383} homozygotes they are nearly entirely absent (Fig. 5e-h, arrows). This phenotype is fully penetrant in the anterior macula (0/11 for mutants; 13/13 wild-type). Similar phenotype is found in *bbs2*^{-/-} mutants (0/9 vs. 7/7, Fig. 5i, j). Posterior macula phenotypes are less consistent. Combined with observations of Cochlin absence in mutant otoliths, these data show that *cep290* and *bbs2* determine the polarity of Cochlin secretion: in wild-type animals, Cochlin is secreted both apically and basally to be incorporated into the otolithic matrix and the basal lamina, respectively. By contrast, in *cep290*^{sa1383} and *bbs2*^{-/-} mutants, Cochlin secretion is

directed basally. In contrast to hair cells, Cochlin-expressing cells do not, however, differentiate prominent cilia (Fig. 5I, Extended data 1). Furthermore, *ovl/Ift88*^{-/-} mutants do not affect Cochlin distribution in the cytoplasm, and we did not see clear defects in two important regulators of apical vesicle trafficking Rab11 and Rab8 in *cep290*^{sa1383} mutants (Extended Data Fig. 9).

Discussion

Our analysis did not detect clear cilia phenotypes in *cep290*^{sa1383} mutants, and our phenotypes were less severe than mouse *cep290* knockouts or zebrafish *cep290*^{h297} mutants, this might be because the *sa1383* allele leaves a substantial amount of protein intact. Additionally, we could not detect significant downregulation of the mutant mRNA using qPCR and we did not detect alternative splicing (Extended data 10), suggesting a truncated protein could be produced. Although our analysis may have missed subtle cilia phenotypes, we consider it more likely that this allele identifies a unique phenotype of CEP290, in addition to novel functions for both Cochlin and a subset of ciliopathy genes. We show that Cochlin determines CaCO₃ crystallization and its role in otolith crystallization may account for vestibular dysfunction associated with human *cochlin* mutations (20, 21). Importantly, the structural defect is only observed in the utricular otoliths, possibly due to the different crystal polymorph composition of the different otoliths. Moreover, Cochlin is enriched basally in sensory epithelia of Meniere's disease patients (27), suggesting that basal secretion defects of Cochlin may also be associated with balance disorders. It is noteworthy that mutation in Cochlin are mostly dominant missense mutations in the N-terminal Factor C homology domain and lead to a form of Cochlin that is secreted but forms deposits in the vestibular and cochlear labyrinths (20, 21). More recently, a form of recessive hearing loss (DFNB110) has been attributed to loss-of-function mutations in Cochlin, similar to the mutations we have generated, and vestibular dysfunction was also reported (28) consistent with our observations.

CEP290 interacts with the BBS complex, which itself is required for IFT particle assembly and transport. The fact that *ovl (ift88)* mutants do not show Cochlin secretion defects is interesting, but consistent with reports that the BBSome has roles in vesicular transport that do not involve cilia. For instance, melanosome transport (29) and Notch receptor recycling to the membrane have been reported (30). Especially the latter suggests that the specific delivery of "Cochlin cargo" to the plasma membrane by the BBSome is an interesting possibility. It is also worth pointing out that *cep290*^{sa1383} and *bbs2*^{-/-} mutants are possibly promising models for slow, age-related degenerative

diseases of the human vestibular system. Few such models are available although they are potentially useful in drug screening efforts.

These results show that ciliary proteins have the ability to act as key regulators of secretory polarity in epithelia. Although epithelial polarity defects have not been reported in vertebrate cilia mutants prior to this analysis (see for example (31, 32)), several studies suggested that ciliogenesis and cell polarity are interconnected. For example, some Nephrocystins interact physically with epithelial polarity determinants Stardust/Pals1 and Par6 (33). Similarly, the Par3/Par6/aPKC complex and Crumbs proteins were shown to contribute to ciliogenesis (34, 35) and several Nephrocystins contribute to tight junction formation in cell culture spheroids (32). We present the first *in vivo* evidence showing that cilia genes facilitate apical secretion and function as potent determinants of secretion polarity (summarized in Fig. 5I). Such a function could be mediated via cytoskeletal elements or by providing secretory vesicle docking sites. Secretion defects reported in this study reveal an entirely new role for cilia genes and suggest that they may regulate secretory processes in other organs and tissues thus contributing to clinical manifestations of human ciliopathies, which have gone unnoticed thus far.

Acknowledgements

We thank Profs. Holley, Johnson, Peden, Marcotti and Smythe for helpful suggestions at various stages of this project. We thank the aquarium staff, the Zebrafish Behavioural Unit and the Electron microscopy facility for their support. This work was supported by Biotechnology and Biological Sciences Research Council (BBSRC, BB/R005192/1; BB/R015457/1), Medical Research Council (MRC, MR/N000714/1)

Figures

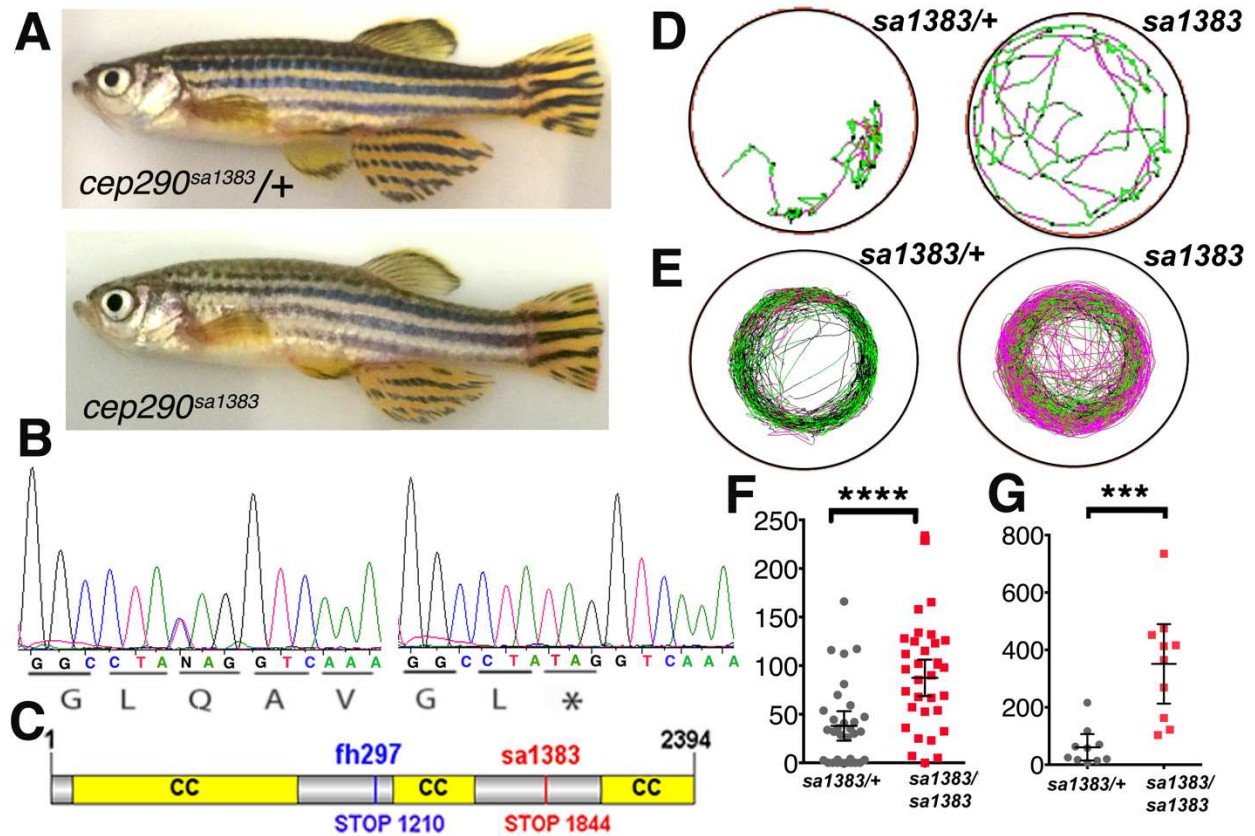


Fig. 1 *cep290* mutant phenotype. **a**, Phenotype of homozygous *cep290*^{sa1383} adult fish. **b**, Sequence of the *sa1383* mutant allele used in this study. **c**, Cep290 domain structure showing mutations used in this study. **d, e**, Example swimming tracks of heterozygote control (left) and homozygous mutant (right) larvae after osmotic shock (**d**) and adults (**e**); black represents slow movement or static, green medium and red fast movement. **f, g**, Total distance traveled for swimming trajectories (mm) such as ones shown in (**d, e**) for larvae after osmotic shock (**f**) and adults (**g**). *****p*<0.0001; *** *p*<0.001, t-test. 95% confidence interval.

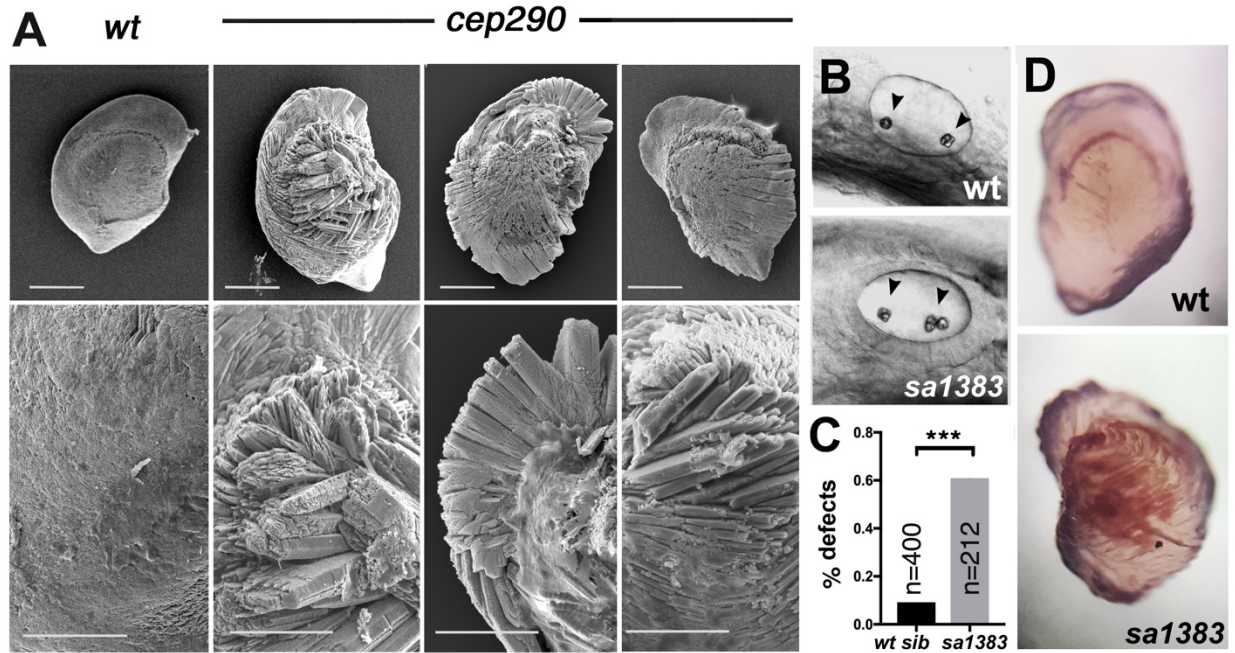


Fig. 2 Otolith crystallization defects in *cep290* mutant homozygotes. **a**, Example SEM images of wild-type and *cep290*^{sa1383} otoliths at 18 months, scale bar 300 μ m. Enlargements in bottom panels, scale bar 150 μ m (n=3). **b**, Side views of otic vesicles in live wild type and *cep290*^{sa1383} homozygous embryos at 36 hpf, the in the posterior ear, in the mutant example, two closely apposed otoliths are seen, where one is expected. Anterior is left, dorsal up, arrowheads indicate otoliths. **c**, Frequency of otolith defects at 36 hpf. p<0.001, chi sq. **d**, Typical example of cobalt nitrate staining of utricular otoliths in wild-type and *cep290*^{sa1383} mutants (n=20).

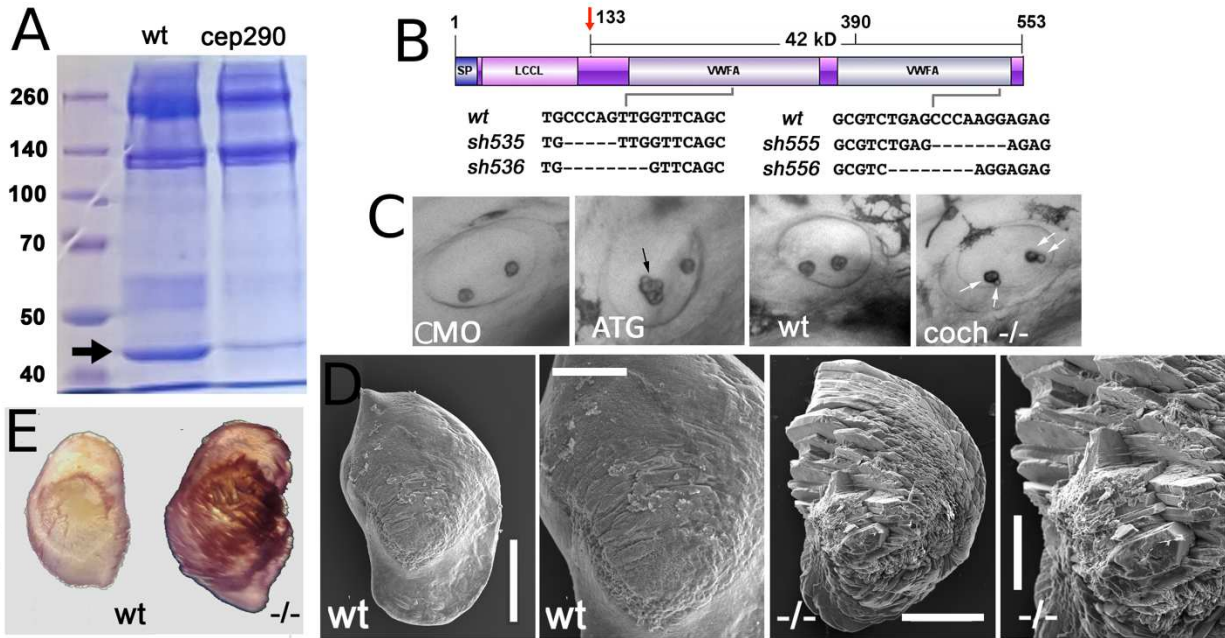


Fig. 3 Otolithic Cochlin deficiency in mutants of cilia genes and *cochlin* mutant phenotype.

a, Otolithic proteins from wild-type and *cep290*^{sa1383} homozygotes separated on a polyacrylamide gel and visualized with Coomassie blue staining. Arrow indicates Cochlin band. **b**, Domain structure of the *cochlin* gene. LCCL, Limulus factor C, Cochlin, Lgl1 domain; vWF, von Willebrand Factor domains. Deletions in CRISPR-induced mutants are indicated. The antiserum against Cochlin was made against the C-terminus (amino acids 390-553) **c**, Otolith morphology in morphant and *coch*^{sh536} mutant embryos as indicated. ATG-targeted morpholino (ATG) was used. Shown are side views of otic vesicles in live embryos, arrows point at otoliths that are abnormal. **d**, SEM of typical otoliths from wild-type and *coch*^{sh536} mutant adult at 7 months of age. Scale bars: Overview 300µm, blow up 150 µm (n=3). **e**, Example of cobalt nitrate staining of utricular otoliths from wild-type and *coch*^{sh536} mutant at 7 months (n=3).

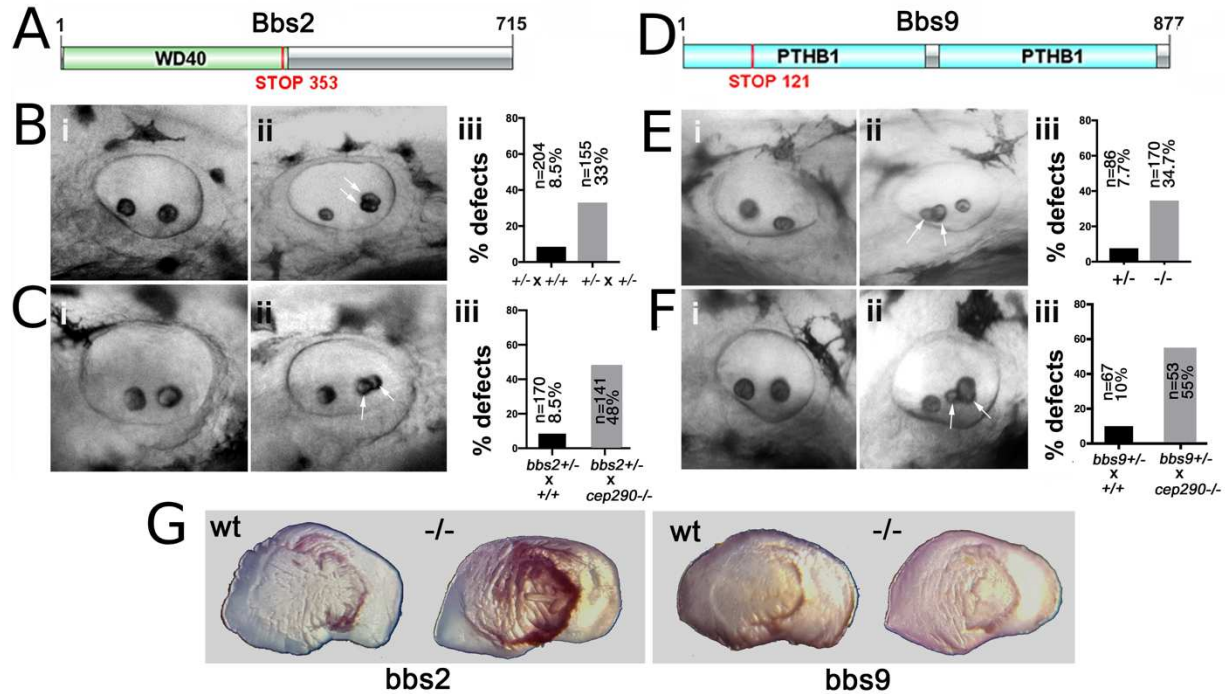


Fig. 4. Otolith phenotypes of BBS mutants and genetic interactions between *cep290* and *bbs* loci at 36 hpf. **a, d** Schematic representation of Bbs2 and Bbs9 protein domain structure. Sites of mutations in *bbs2*^{sa2952} and *bbs9*^{sa14425} alleles used in this study are indicated. **b**, *bbs2*^{-/-} mutant phenotype. Lateral views of otic vesicles from **(i)** *bbs2*^{+/-} outcross to a wild-type strain and **(ii)** *bbs2*^{+/-} incross. In **(ii)** an individual with abnormal otolith morphology is shown. **(iii)** Frequency of otolith defects in embryos originating from *bbs2*^{+/-} outcross and incross as above. ($p < 0.0001$, χ^2 test) **c**, Phenotype of embryos originating from *bbs2*^{+/-} outcrosses to a wild-type and a *cep290*^{-/-} strain. Lateral views of otic vesicles from **(i)** *bbs2*^{+/-} outcross to a wild-type strain and **(ii)** *bbs2*^{+/-} outcross to *cep290*^{sa1383} homozygous strain. **(iii)** Frequency of otolith defects in *bbs2*^{+/-} outcrosses as above. ($p < 0.0001$, χ^2 test). **e**, Phenotype of *bbs9*^{-/-} mutant homozygotes. Lateral views of the otic vesicle from **(i)** *bbs9*^{+/-} heterozygote and **(ii)** *bbs9*^{-/-} mutant homozygote with abnormal otolith number (3 instead of 2). **(iii)** Frequency of otolith defects in *bbs9*^{-/-} homozygotes, compared to *bbs9*^{+/-} heterozygotes. ($p < 0.0001$, χ^2 test). **f**, Phenotype of embryos originating from *bbs9*^{+/-} outcrosses to a wild-type and a *cep290*^{-/-} strain. Lateral views of otic vesicles from **(i)** *bbs9*^{+/-} outcross to a wild-type and **(ii)** *bbs9*^{+/-} outcross to *cep290*^{-/-} homozygous strain. **(iii)** Frequency of otolith defects in *bbs9*^{+/-} outcrosses as above. ($p < 0.0001$, χ^2 test). Arrows indicate abnormally forming otoliths. **g**, Examples of cobalt nitrate staining of

utricle otoliths from *bbs2*^{-/-} (h) and *bbs9*^{-/-} (i) mutants at 23 and 26 months of age, respectively (n=3).

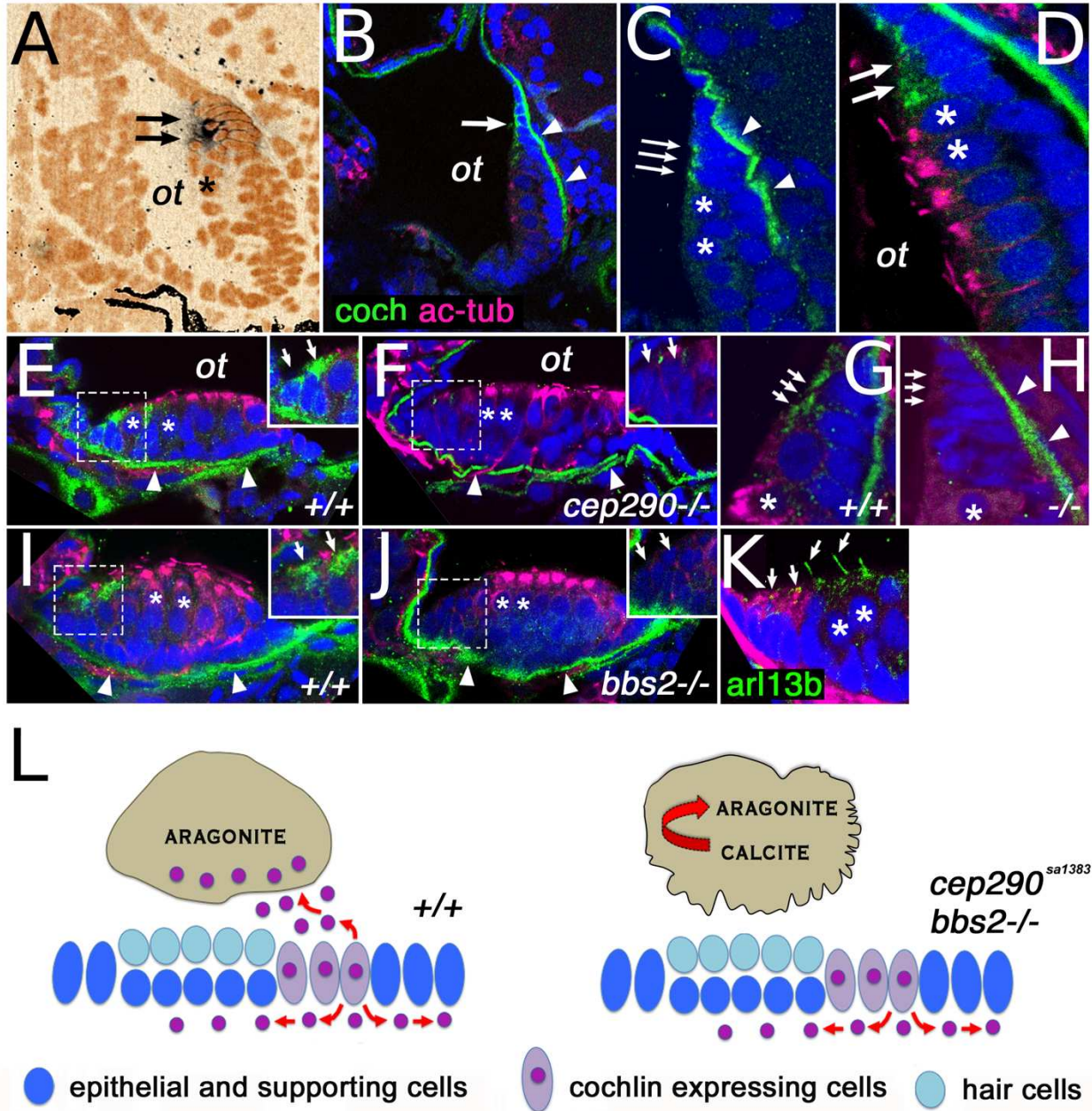


Fig. 5 Cochlin expression pattern. a, *cochlin* transcript expression (arrows) in the posterior macula of the zebrafish otic vesicle at 5 dpf. b, c, Cochlin protein expression (in green) in the posterior macula at 5 dpf. d, Cochlin expression (in green, arrows) at the dorsal rim of the posterior macula in cells immediately adjacent to hair cells (asterisks). e-h, Cochlin protein localization in anterior (e, f) and posterior (g, h) maculae of wild-type and *cep290*^{sa1383} homozygotes as indicated

at 5 dpf. **i, j**, Cochlin expression in the anterior macula of wild-type (**i**) and *bbs2*^{-/-} mutants (**j**). **k**, Cilia visualized with Arl13b-GFP transgene (in green, arrows), Cochlin in red. **l**, Model of *cep290* and *bbs2* function in Cochlin secretion. Loss of *cep290*, *bbs2* and most likely other cilia-related genes leads to defects apical Cochlin secretion into the ear lumen and causes abnormal crystallization of otolithic calcium carbonate. In (**d-k**) sections are double stained for acetylated tubulin (in magenta), which accumulates apically in hair cells. All sections are counterstained with DAPI in blue (pseudocolored in orange in **a**). Insets in (**e, f, i, j**) show enlargements of Cochlin secreting cells (enclosed in dashed line boxes). In (**b-j**) arrows indicate Cochlin secreting cells, arrowheads point to Cochlin presence in the basal lamina. “ot” otolith position, asterisks indicate hair cells. CaCO₃ crystal structure after (36)

1. D. A. Parfitt *et al.*, Identification and Correction of Mechanisms Underlying Inherited Blindness in Human iPSC-Derived Optic Cups. *Cell Stem Cell* **18**, 769-781 (2016).
2. F. Coppieters, S. Lefever, B. P. Leroy, E. De Baere, CEP290, a gene with many faces: mutation overview and presentation of CEP290base. *Hum Mutat* **31**, 1097-1108 (2010).
3. H. Straka, A. Zwergal, K. E. Cullen, Vestibular animal models: contributions to understanding physiology and disease. *J Neurol* **263 Suppl 1**, S10-23 (2016).
4. S. Fermani, S. Vanzo, M. Miletic, G. Zaffino, Influence on the Formation of Aragonite or Vaterite by Otolith Macromolecules. *European Journal of Inorganic Chemistry* **2005**, 162-167 (2005).
5. R. Dongni, G. Yonghua, F. Qingling, Comparative study on nano-mechanics and thermodynamics of fish otoliths. *Mater Sci Eng C Mater Biol Appl* **33**, 9-14 (2013).
6. C. Sollner *et al.*, Control of crystal size and lattice formation by starmaker in otolith biomineralization. *Science* **302**, 282-286 (2003).
7. J. Weigele, T. A. Franz-Odenaal, R. Hilbig, Not All Inner Ears are the Same: Otolith Matrix Proteins in the Inner Ear of Sub-Adult Cichlid Fish, *Oreochromis Mossambicus*, Reveal Insights Into the Biomineralization Process. *Anat Rec (Hoboken)* **299**, 234-245 (2016).
8. G. Ishiyama, I. A. Lopez, A. R. Sepahdari, A. Ishiyama, Meniere's disease: histopathology, cytochemistry, and imaging. *Ann N Y Acad Sci* **1343**, 49-57 (2015).
9. I. S. Curthoys, L. Manzari, Otolithic disease: clinical features and the role of vestibular evoked myogenic potentials. *Semin Neurol* **33**, 231-237 (2013).
10. M. Tsujikawa, J. Malicki, Intraflagellar transport genes are essential for differentiation and survival of vertebrate sensory neurons. *Neuron* **42**, 703-716 (2004).
11. K. J. Clark, N. J. Boczek, S. C. Ekker, Stressing zebrafish for behavioral genetics. *Rev Neurosci* **22**, 49-62 (2011).
12. E. Leventea, K. Hazime, C. Zhao, J. Malicki, Analysis of cilia structure and function in zebrafish. *Methods Cell Biol* **133**, 179-227 (2016).

13. D. Inoue, J. Wittbrodt, One for all--a highly efficient and versatile method for fluorescent immunostaining in fish embryos. *PLoS One* **6**, e19713 (2011).
14. B. Thisse *et al.*, Spatial and temporal expression of the zebrafish genome by large-scale in situ hybridization screening. *Methods Cell Biol* **77**, 505-519 (2004).
15. M. Gering, R. Patient, Hedgehog signaling is required for adult blood stem cell formation in zebrafish embryos. *Dev Cell* **8**, 389-400 (2005).
16. J. Malicki, H. Jo, X. Wei, M. Hsiung, Z. Pujic, Analysis of gene function in the zebrafish retina. *Methods* **28**, 427-438 (2002).
17. T. T. Whitfield, Cilia in the developing zebrafish ear. *Philos Trans R Soc Lond B Biol Sci* **375**, 20190163 (2020).
18. B. B. Riley, C. Zhu, C. Janetopoulos, K. J. Aufderheide, A critical period of ear development controlled by distinct populations of ciliated cells in the zebrafish. *Dev Biol* **191**, 191-201 (1997).
19. B. F. Py *et al.*, Cochlin produced by follicular dendritic cells promotes antibacterial innate immunity. *Immunity* **38**, 1063-1072 (2013).
20. N. G. Robertson, S. A. Hamaker, V. Patriub, J. C. Aster, C. C. Morton, Subcellular localisation, secretion, and post-translational processing of normal cochlin, and of mutants causing the sensorineural deafness and vestibular disorder, DFNA9. *J Med Genet* **40**, 479-486 (2003).
21. N. G. Robertson *et al.*, Mutations in a novel cochlear gene cause DFNA9, a human nonsyndromic deafness with vestibular dysfunction. *Nat Genet* **20**, 299-303 (1998).
22. U. Khetarpal, H. F. Schuknecht, R. R. Gacek, L. B. Holmes, Autosomal dominant sensorineural hearing loss. Pedigrees, audiologic findings, and temporal bone findings in two kindreds. *Arch Otolaryngol Head Neck Surg* **117**, 1032-1042 (1991).
23. S. M. Jones *et al.*, Hearing and vestibular deficits in the Coch(-/-) null mouse model: comparison to the Coch(G88E/G88E) mouse and to DFNA9 hearing and balance disorder. *Hear Res* **272**, 42-48 (2011).
24. Y. Zhang *et al.*, BBS mutations modify phenotypic expression of CEP290-related ciliopathies. *Hum Mol Genet* **23**, 40-51 (2014).
25. T. R. Stowe, C. J. Wilkinson, A. Iqbal, T. Stearns, The centriolar satellite proteins Cep72 and Cep290 interact and are required for recruitment of BBS proteins to the cilium. *Mol Biol Cell* **23**, 3322-3335 (2012).
26. H. Jin *et al.*, The conserved Bardet-Biedl syndrome proteins assemble a coat that traffics membrane proteins to cilia. *Cell* **141**, 1208-1219 (2010).
27. A. P. Calzada, I. A. Lopez, L. Beltran Parrazal, A. Ishiyama, G. Ishiyama, Cochlin expression in vestibular endorgans obtained from patients with Meniere's disease. *Cell Tissue Res* **350**, 373-384 (2012).
28. S. P. F. JanssensdeVarebeke *et al.*, Bi-allelic inactivating variants in the COCH gene cause autosomal recessive prelingual hearing impairment. *Eur J Hum Genet* **26**, 587-591 (2018).
29. H. J. Yen *et al.*, Bardet-Biedl syndrome genes are important in retrograde intracellular trafficking and Kupffer's vesicle cilia function. *Hum Mol Genet* **15**, 667-677 (2006).
30. C. C. Leitch, S. Lodh, V. Prieto-Echague, J. L. Badano, N. A. Zaghoul, Basal body proteins regulate Notch signaling through endosomal trafficking. *J Cell Sci* **127**, 2407-2419 (2014).

31. Y. Omori *et al.*, Elipsa is an early determinant of ciliogenesis that links the IFT particle to membrane-associated small GTPase Rab8. *Nat Cell Biol* **10**, 437-444 (2008).
32. L. Sang *et al.*, Mapping the NPHP-JBTS-MKS protein network reveals ciliopathy disease genes and pathways. *Cell* **145**, 513-528 (2011).
33. M. Delous *et al.*, Nephrocystin-1 and nephrocystin-4 are required for epithelial morphogenesis and associate with PALS1/PATJ and Par6. *Hum Mol Genet* **18**, 4711-4723 (2009).
34. S. Fan *et al.*, Polarity proteins control ciliogenesis via kinesin motor interactions. *Curr Biol* **14**, 1451-1461 (2004).
35. K. Hazime, J. J. Malicki, Apico-basal Polarity Determinants Encoded by crumbs Genes Affect Ciliary Shaft Protein Composition, IFT Movement Dynamics, and Cilia Length. *Genetics* **207**, 1041-1051 (2017).
36. V. Blanco-Gutierrez, A. Demourgues, V. Jubera, M. Gaudon, Eu(iii)/Eu(ii)-doped (Ca_{0.7}Sr_{0.3})CO₃ phosphors with vaterite/calcite/aragonite forms as shock/temperature detectors. *Journal of Materials Chemistry C* **2**, 9969-9977 (2014).

Supplementary Figures

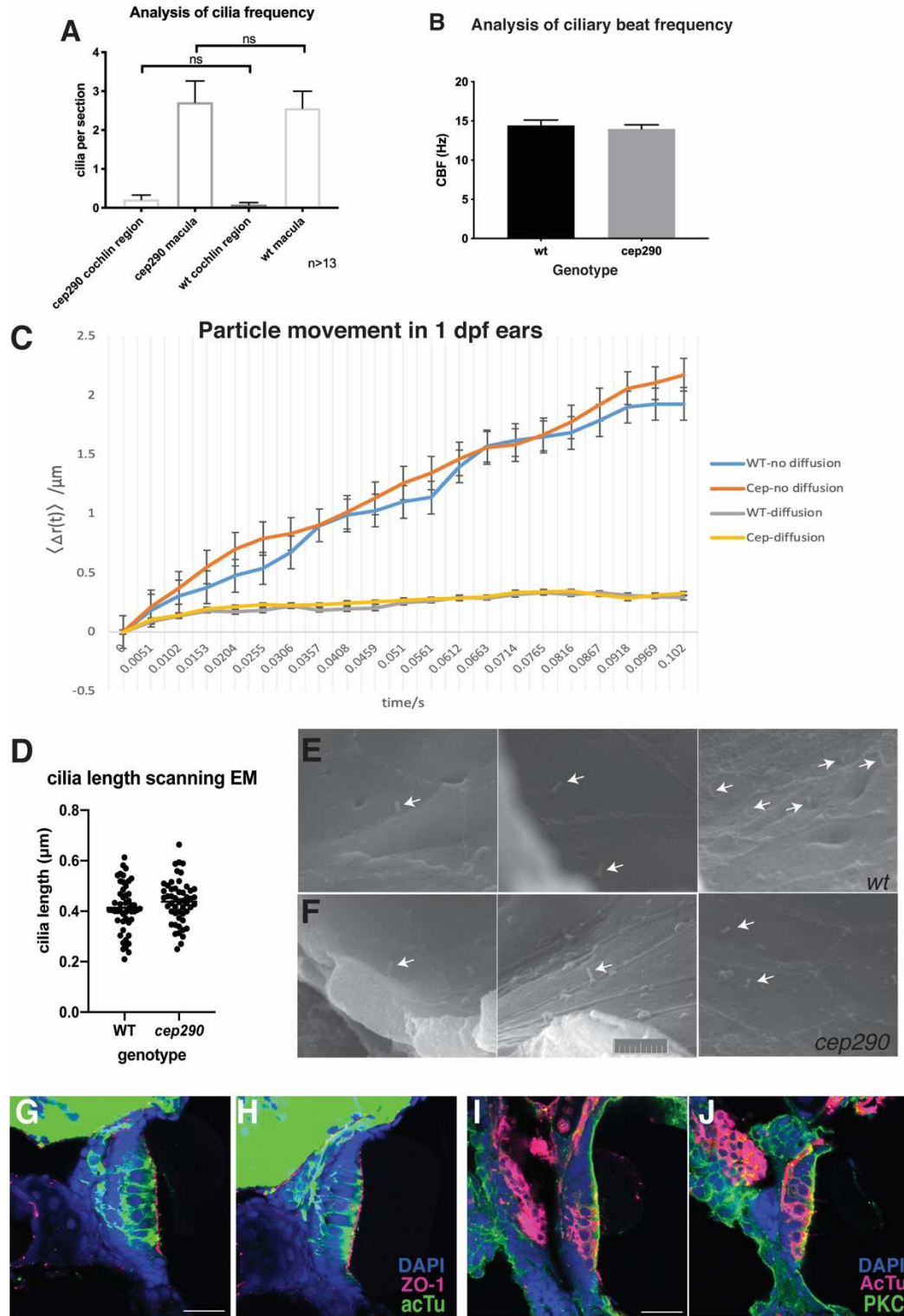
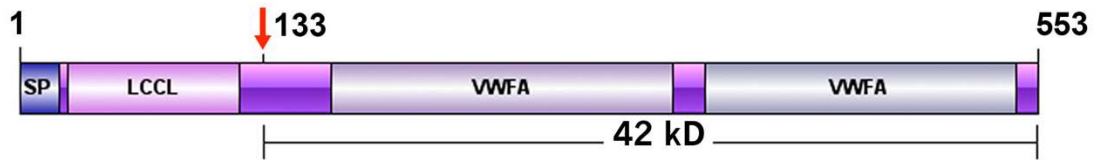


Fig. S1 (A) Counts of hair cell associated on sections with maculae, or cochlin expression regions in WT and *cep290*^{sa1383}. In both genotypes, hair cells are only rarely associated with high cochlin expressing regions ($p < 0.001$, $n > 13$, Kruskal-Wallis), no different

between genotypes is observed. **(B)** Ciliary functional analysis of the early stage (20hpf) ear development in embryonic zebra fish at 28°C. There was no significant difference ($p=0.6$; unpaired Student's t-test, $n=10$ for WT and 19 for *cep290*) between wild type (black fill) and the *cep290^{sa1383}* (grey fill) embryos. See supplemental Movies S1 and S2 for examples. The cilia from both groups displayed a clockwise rotational beat pattern. Pre-otolith aggregation was observed equally in both groups. Particle movement by the cilia was also equally observed in the 2 groups using real time video microscopy. **(C)** Analysis of particle displacement in 1dpf ears, we analysed both particles near motile cilia (no diffusion) and passively moving particles distant from such cilia (diffusion); $n=16$. In both genotypes particles moved in a similar manner. **(D)** Measurement of cilia length at 4.5-5dpf larvae in SEM images, no significant difference was observed ($p=0.18$ unpaired t-test, $n=49$ from >4 larvae per genotype). Representative SEM images of wild-type **(E)** and *cep290^{sa1383}* mutants **(F)**, showing cilia (white arrows) emanating from the epithelium lining the semi-circular canals. Posterior macula of WT, scale bar 2 μ m **(G)** and *cep290^{sa1383}* **(H)** mutants, stained with DAPI (blue), ZO-1 (magenta) and acetylated Tubulin (green) showing normal apical labelling in mutants. Anterior macula of WT **(I)** and *cep290^{sa1383}* **(J)** mutants, stained with DAPI (blue), acetylated Tubulin (magenta) and aPKC (green) showing normal apical labelling in mutants **G-J**: scale bars 20 μ m.



>B3DFV8_B3DFV8_DANRE Coagulation factor C homolog, cochlin

MSLWFAVLHV LGILSLSWCT SGSELVNATP ISCGTRAVDL SDTHLLVLCP ANCSLWLSLV FGSGVYASIS SICGAAIHRG IIGLSGGPVE VHGLQGRNTY
 LSSYAHGVQS QLSLQWSASF TVARTISLPL EVSSQTSSSA TVASGAAKKP VKKIVKKPPP ATAHKDCPVD MALLLDSSYN IGQRRFNLQK NFVSKLATML
 KVGQTQGPVHG VVQTSETPRT EFYLTNYTTA KDVTFAIKEI PYIGGNTNTG KAILHTVRNF FSPDFGVRRG YPRVIVVFVD GWPSDNVEEA AILARESGIN
 IFFVSVAKPS PEEASLVSDQ DFMRKAVCKD NEFFFTMPS WFSTNKFVKP LAQKLC SIDQ MLCSKTCYNS VDLGFLIDGS SSVGDGNFRL VLDLLVSIAR
 SFDISDIGSR IGAIQFTYDQ RMEFNFNDHV LKDNALRALQ KIPYMSGGTA TGDAINFAVR SLFKPRSSSN RKFLIIITDG QSYDDVRVPA MAAQREGITV
 YAVGVAWAPM EDLKAMASEP KESHVFFTRE FTGLGQFQQP IVRGICRDFT EFN

MSLWFAVLHV LGILSLSWCT SGSELVNATP ISCGTRAVDL SDTHLLVLCP ANCSLWLSLV FGSGVYASIS SICGAAIHRG IIGLSGGPVE VHGLQGRNTY
 LSSYAHGVQS QLSLQWSASF TVARTISLPL EVSSQTSSSA TVASGAAKKP VKKIVKKPPP ATAHKDCPVD MALLLDSSYN IGQRRFNLQK NFVSKLATML
 KVGQTQGPVHG VVQTSETPRT EFYLTNYTTA KDVTFAIKEI PYIGGNTNTG KAILHTVRNF FSPDFGVRRG YPRVIVVFVD GWPSDNVEEA AILARESGIN
 IFFVSVAKPS PEEASLVSDQ DFMRKAVCKD NEFFFTMPS WFSTNKFVKP LAQKLC SIDQ MLCSKTCYNS VDLGFLIDGS SSVGDGNFRL VLDLLVSIAR
 SFDISDIGSR IGAIQFTYDQ RMEFNFNDHV LKDNALRALQ KIPYMSGGTA TGDAINFAVR SLFKPRSSSN RKFLIIITDG QSYDDVRVPA MAAQREGITV
 YAVGVAWAPM EDLKAMASEP KESHVFFTRE FTGLGQFQQP IVRGICRDFT EFN

MSLWFAVLHV LGILSLSWCT SGSELVNATP ISCGTRAVDL SDTHLLVLCP ANCSLWLSLVFGSGVYASIS SICGAAIHRG IIGLSGGPVE VHGLQGRNTY
 LSSYAHGVQS QLSLQWSASF TVARTISLPL EVSSQTSSSA TVASGAAKKP VKKIVKKPPP ATAHKDCPVD MALLLDSSYN IGQRRFNLQK NFVSKLATML K
VGTQGPVHG VVQTSETPRT EFYLTNYTTA KDVTFAIKEI PYIGGNTNTG KAILHTVRNF FSPDFGVRRG YPRVIVVFVD GWPSDNVEEA AILARESGINIF
FVSVAKPS PEEASLVSDQ DFMRKAVCKD NEFFFTMPS WFSTNKFVKP LAQKLC SIDQ MLCSKTCYNS VDLGFLIDGS SSVGDGNFRL VLDLLVSIAR SF
DISDIGSR IGAIQFTYDQ RMEFNFNDHV LKDNALRALQ KIPYMSGGTA TGDAINFAVR SLFKPRSSSN RKFLIIITDG QSYDDVRVPA MAAQREGITV YAV
GVAWAPM EDLKAMASEP KESHVFFTRE FTGLGQFQQP IVRGICRDFT EFN

Fig. S2 Peptide coverage obtained in mass spectrometry experiments. Recovered peptides are underlined and in green type. Vertical arrow indicates the cleavage site between LCCL and VWF domains. Note that peptide coverage of the LCCL domain is low, compared to the rest of the protein. Results from three experimental repeats are shown.

a >NP_001003823.1 cochlin precursor [Danio rerio]

MSLWFAVLHVLGILSLSWCTSGSELNVATPISCGTRAVDLSDTHLLVLCPANCSLWLSLVFGSG
 VYASISSICGAAIHRGIIGLSGGPVEVHGLQGR^{TNYLSS}YAHGVQSQSLSQWSASFTVARTISL
 PL^{EV}SSQTSSSAIVASGAAKKPVKKIVKKPPPATAHKD^{CPVDMALLDSSYNTGQRRP}FLQKNF
 VSKLATMLKVG^{TQ}GPVGVV^{QT}SETPRTEFYLTNYTTAKDVTFAIKEIPYIGGNTNTGKAILHT
 VRNFFSPDFG^{VRRGY}PRVIVFVDGWPSDNVEEAAILARESGINIFFVSVAKPSPEEASLVSDQ
 DFM^{RKAVCKD}NEFFFTT^{MPSWF}STNKFVKPLA^{QKL}CSIDQMLCSKTCYNSVDLGLFDGSSSVG
 DGNFRLVLDLLVSIARSFDISDIGSRIGAIQFTYDQ^{RMEFNF}N^{DHVLK}DNALRALQKIPYMSGG
 TATGDAINFAVRS^{LFKPRSS}NRKFLIIITDGQSYDDV^{RV}PAMAAQREGITVYAVGVAVAPMED
 LKAMASEPKESHVFF^{TREFT}TGLGQFQ^{QPI}VRGICRDFTEFN

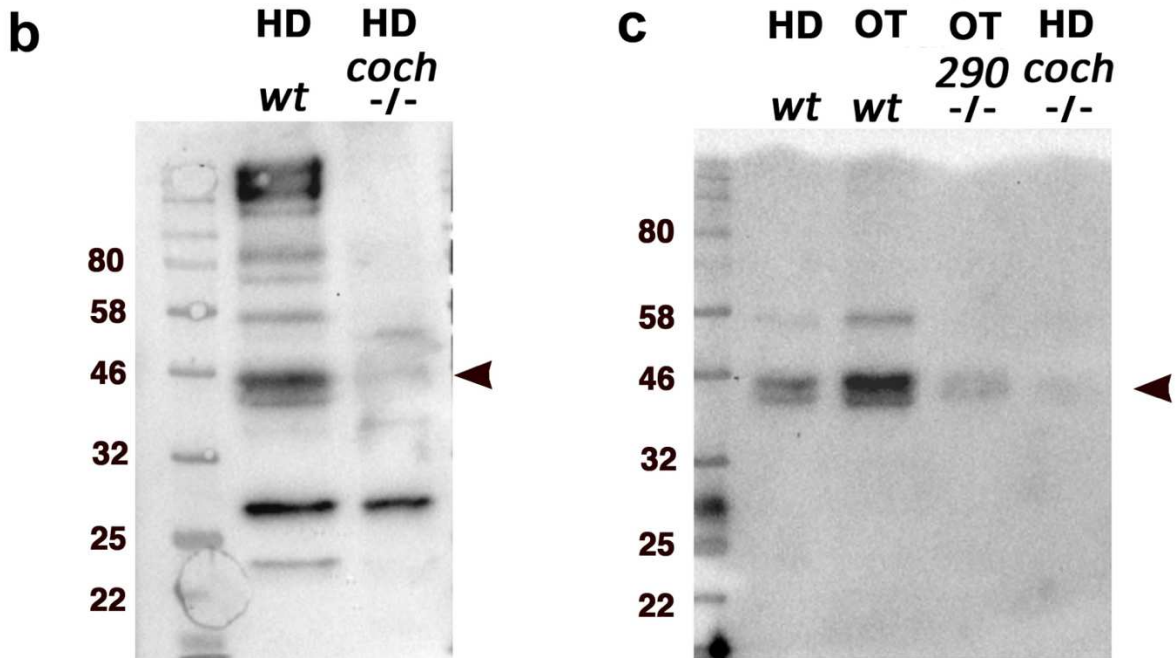


Fig. S3 Zebrafish cochlin protein sequence. (A) The LCCL domain is underlined, VWF domains are in blue. Peptide used to generate antibody is highlighted in green. Protein sequence used to generate antibody to 6xHis-fusion is highlighted in yellow. The latter antibody was used for subsequent IHC stainings. Cochlin cleavage site is in red. (B) Western blots using anti-peptide antibody (C) anti-His-tag fusion (right). Genotypes and tissues are indicated above each blot. Arrowhead indicates the Cochlin band. HD, whole head. OT, otolith.

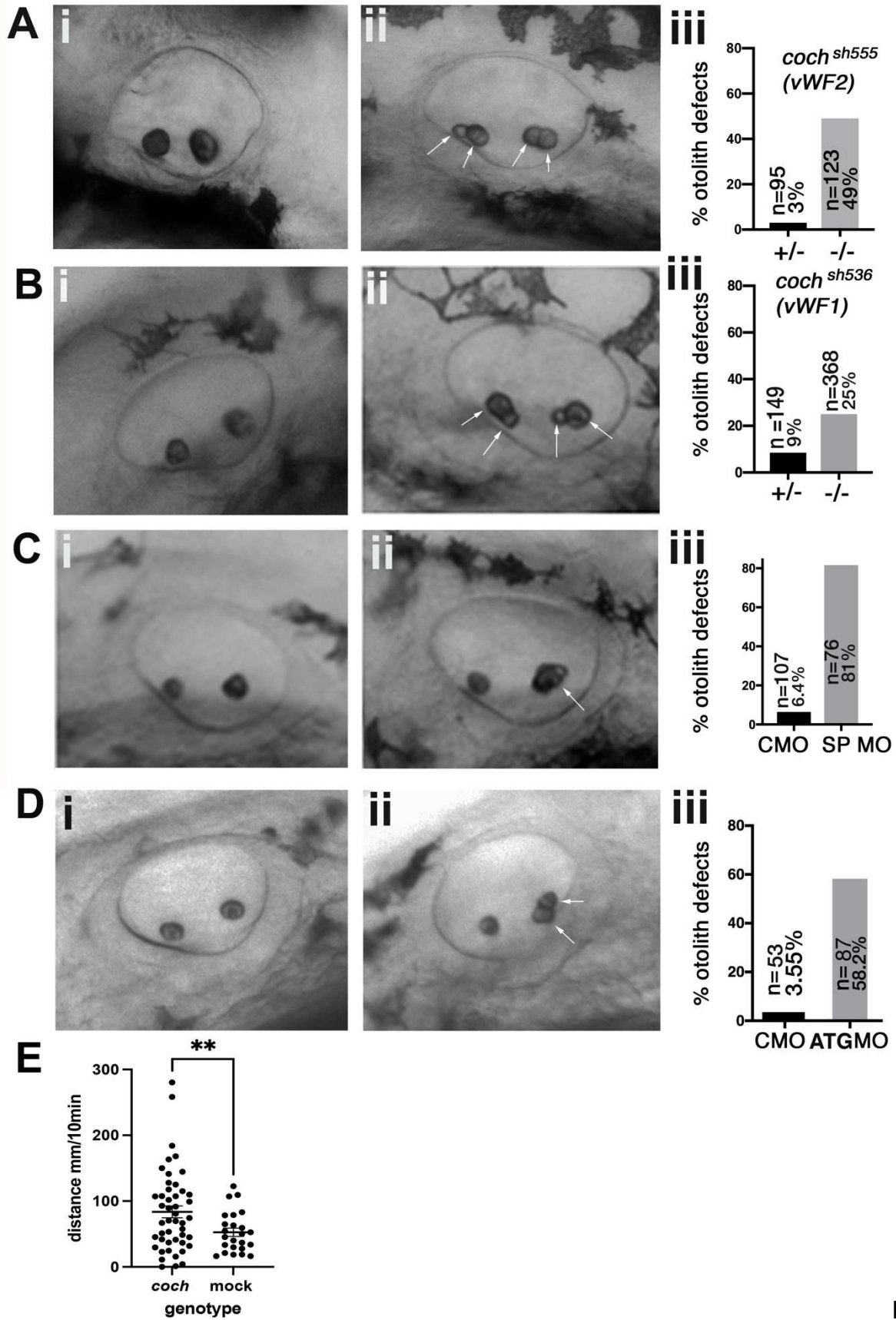


Fig.

S4 Embryonic *cochlin* otolith phenotype at 36 hpf and behavioural phenotype at

d5.2. (A) Phenotype of embryos with mutations in the second vWF domain. Lateral views of the otic vesicle of (i) heterozygous and (ii) homozygous mutant *coch*^{sh555} zebrafish embryo. (iii) Frequency of otolith defects in *coch*^{sh555} homozygotes compared to *coch*^{sh555/+} heterozygotes ($p < 0.0001$, χ^2 test). **(B)** Phenotype of embryos with mutation in the first vWF domain. Lateral views of the otic vesicle of (i) heterozygous and (ii) homozygous mutant *coch*^{sh536} embryo. (iii) Frequency of otolith defects in *coch*^{sh536} mutants compared to heterozygotes ($p < 0.0001$, χ^2 test). **(C)** Phenotype of *cochlin* morphants induced with anti-splice site morpholino. Lateral views of the otic vesicle in (i) control morpholino and (ii) anti-splice site morpholino treated embryos. (iii) Frequency of otolith defects in control and morphant animals induced with anti splice site morpholino ($p < 0.0001$, χ^2 test). **(D)** Phenotype of *cochlin* morphants induced with anti-ATG morpholino. Lateral views of the otic vesicle in (i) control morpholino and (ii) anti-ATG morpholino treated embryos. (iii) Frequency of otolith defects in control and morphant animals induced with anti-ATG morpholino ($p < 0.0001$, χ^2 test). Arrows denote abnormally forming otoliths. **(E)** Analysis of total distance travelled of *cochlin* crispants and mock (Cas9) injected embryos at 5.2dpf, ** $p < 0.01$ $n=47$ and 24 resp., T-test with Welch's correction.

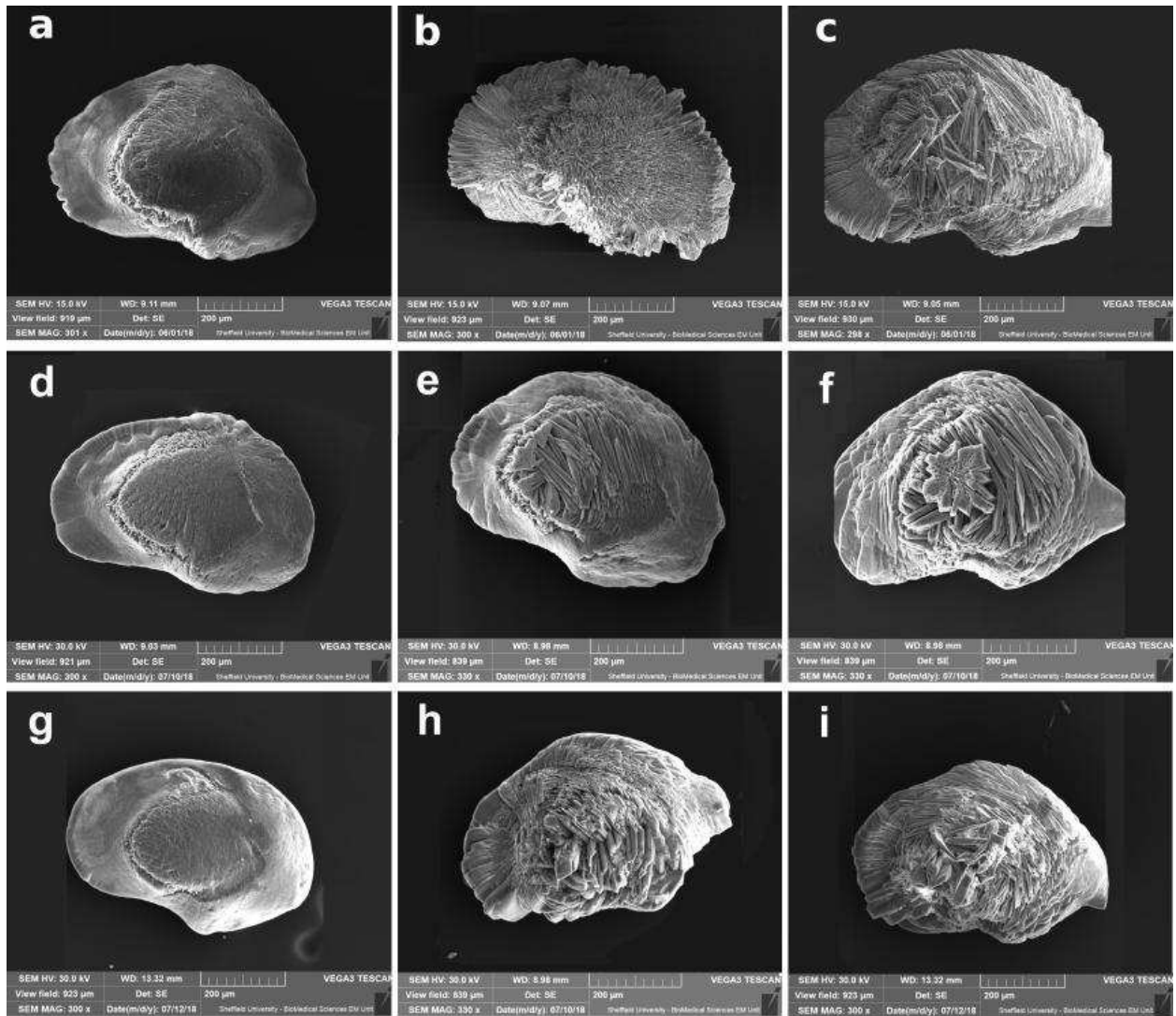


Fig. S5 Otolith morphology in adult cochlin mutant homozygotes. Scanning electron micrographs of otoliths from wild-type (**A, D, G**), *coch^{sh536}* homozygotes (**B, C, E, F**) and *coch^{sh555}* homozygotes (**H, I**) at 8 months of age. Scale bar, 200µm.

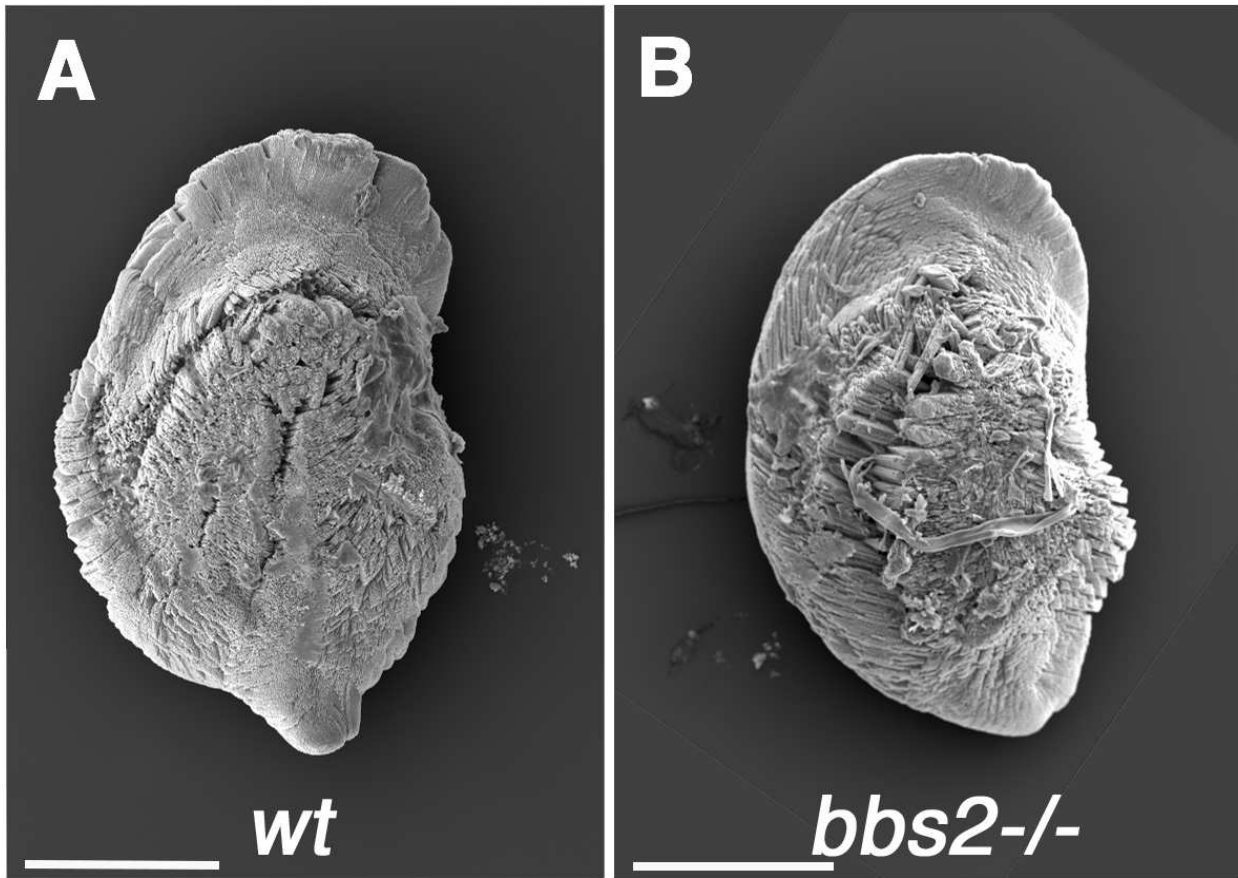


Fig. S6 Otolith phenotype in adult *bbs2*^{-/-} mutants. Scanning electron micrograph of otoliths from wild-type (A) and *bbs2*^{-/-} mutant (B) homozygote at 2.4 years of age. Scale bar, 200 μ m.

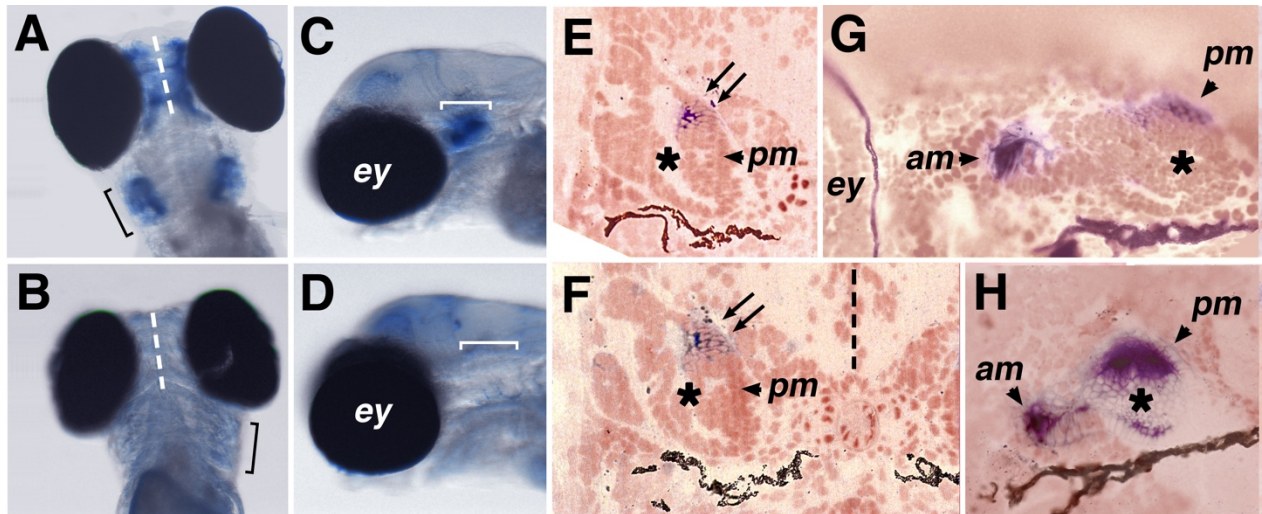


Fig. S7 Cochlin transcript expression. (A-D) Images of zebrafish following whole-mount in situ hybridization with anti-sense (A, C) and sense (B, D) *cochlin* probes at 5 dpf. Brackets show the position of the ear. (E-H) Plastic sections through zebrafish ears following in situ hybridization with a *cochlin* probe at 5 dpf. Shown are transverse (E, F) and longitudinal (G, H) sections. Asterisks indicate ear lumen. Arrows in (E, F) point to *cochlin* expression (blue signal). Sections were counterstained with DAPI (pseudo colored in pink). am, anterior macula. pm, posterior macula. ey, eye.

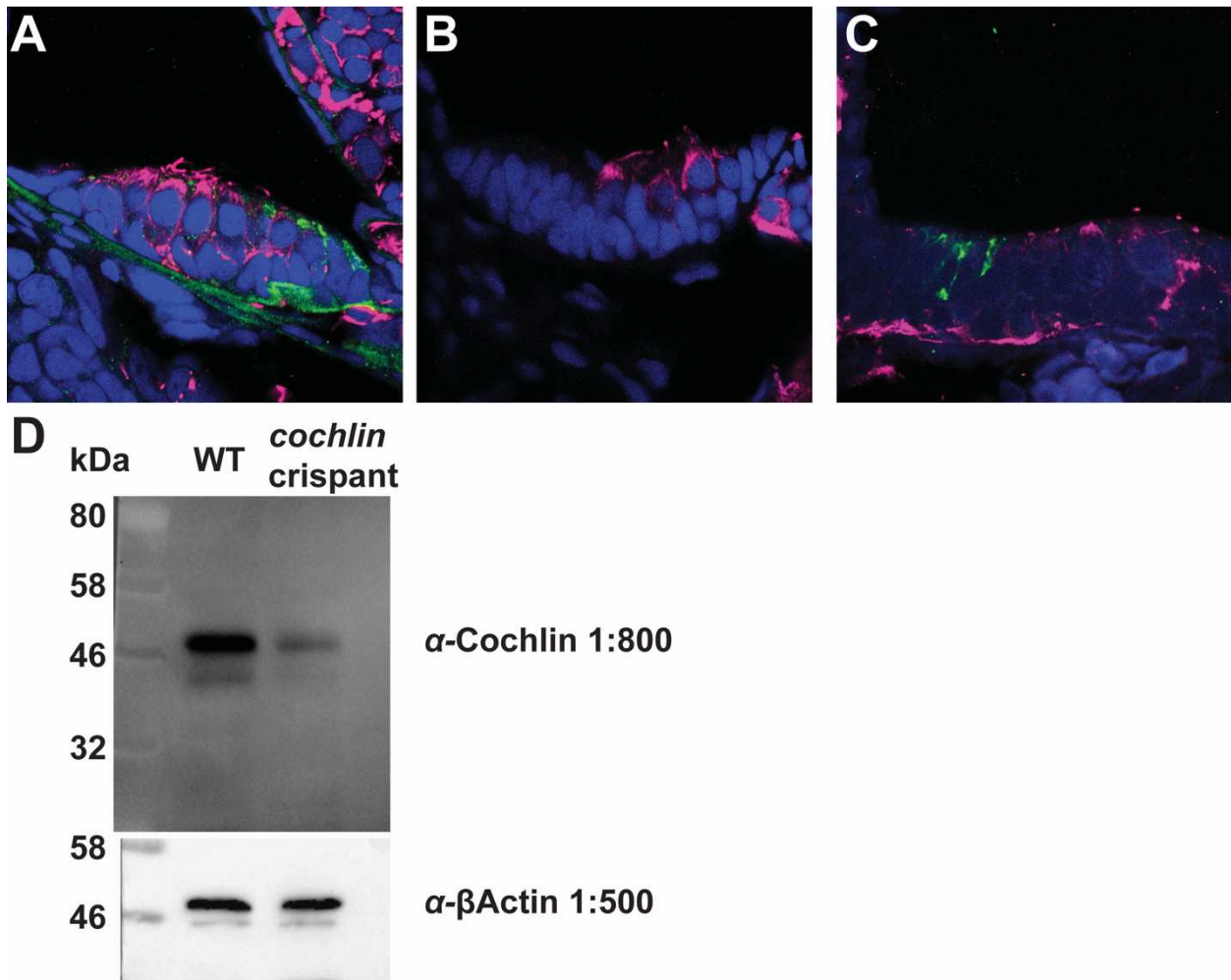


Fig. S8 (A) Uninjected control section showing clear apical Cochlin staining (green) in the cells adjacent to the macula. (B) Cochlin crisprant without detectable staining for Cochlin, showing specificity of the Coch antibody. Due to the stochastic nature of CRISPR activity, crisprant may lead to mosaics where some cells will still express the protein whereas others do not, an example like this is shown in (C) and can provide an internal control for successful antibody staining. In A-C acetylatedTubulin is shown in magenta (D) Western Blot analysis of pools of 15 embryos stained with α-Cochlin antibody and a loading control (α-βActin) confirming a reduction in Cochlin expression

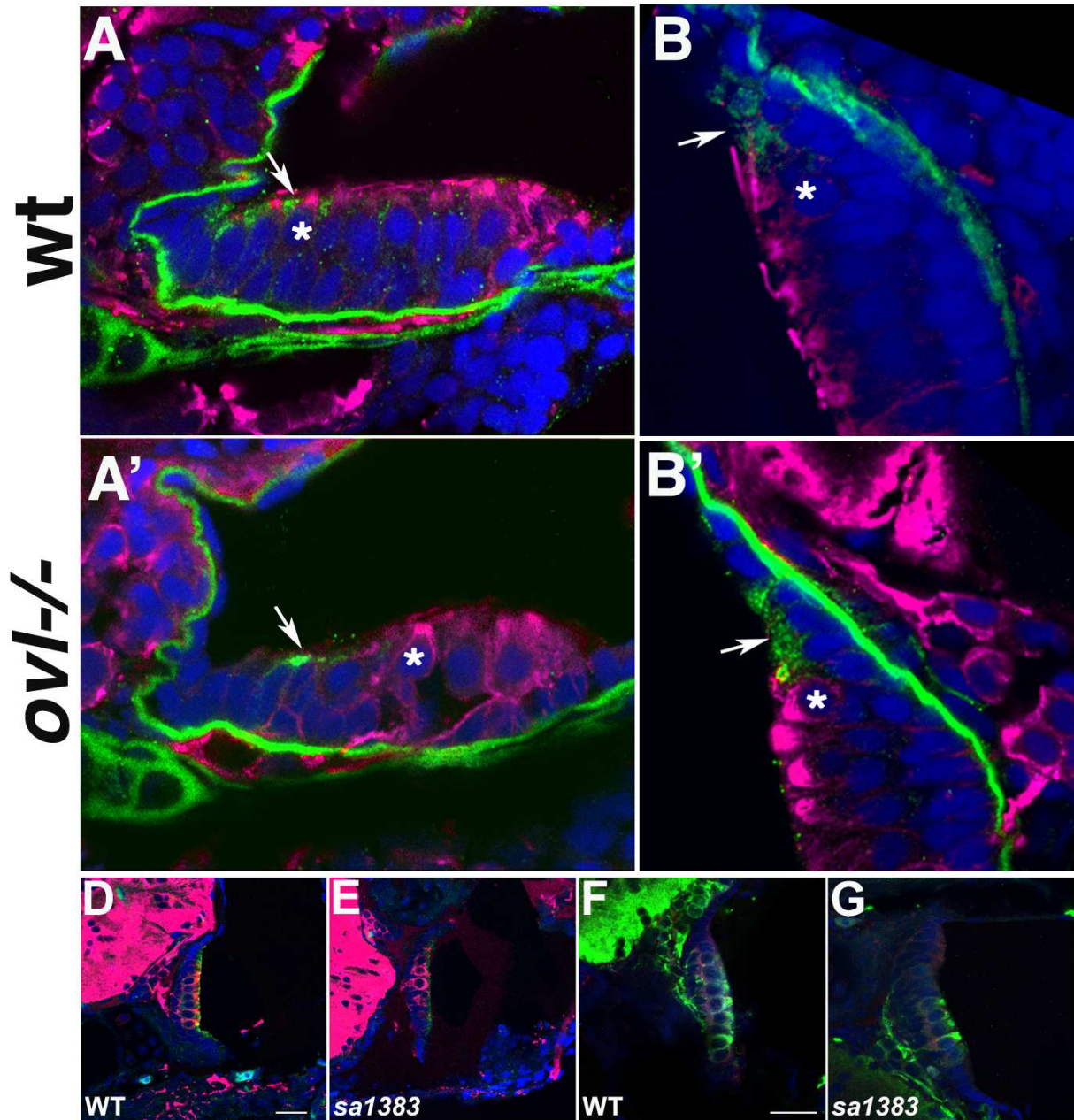


Fig. S9 Cochlin expression in *ovl* mutants, Rab11 Rab8 labeling of *cep290*^{sa1383} mutants. Confocal images of cryosections of the anterior (**A, A'**) and posterior (**B, B'**) macula at 5 dpf stained with anti-Cochlin (green) and anti-acetylated-tubulin (magenta) antibodies. Embryos are derived either from *ovl*^{-/+} outcross to a wild type strain (**A, B**) or from *ovl*^{-/-} incross and are homozygous for *ovl*^{-/-} mutant allele (**A', B'**). Arrows point to Cochlin expression while asterisks show an example of a hair cell. Nuclei are stained with DAPI. (**D,E**) Confocal images of anterior macula at 5dpf labeled with anti-Rab11

(green) and anti-acetylated tubulin (magenta) in *cep290^{sa1383}* mutants and wild-type embryos. (F,G) Confocal images of anterior macula at 5dpf labeled with anti-Rab8 (magenta) and anti-acetylated tubulin (green) in *cep290^{sa1383}* mutants and wild-type embryos. Scale bar 20 μ m

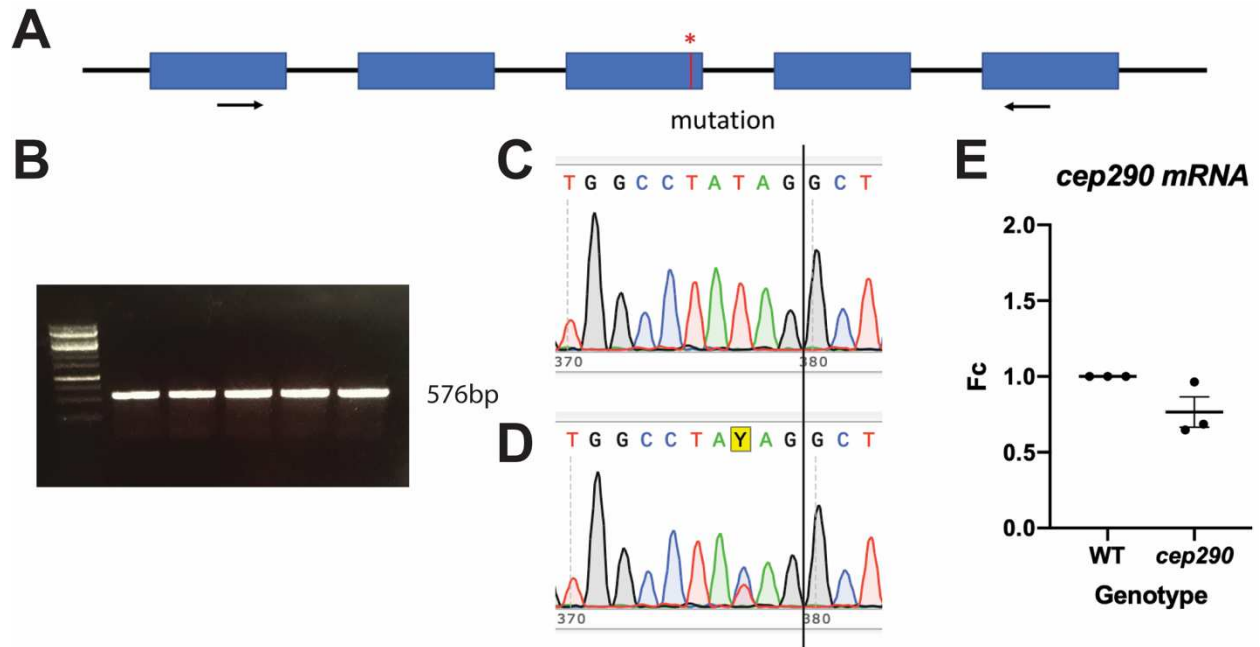


Fig. S10 Expression analysis of *cep290^{sa1383}*. (A) schematic showing primer position for analysis of splicing and expression analysis, forward primer CTTGTGGAGCGCTTGAAGAA reverse primer ACCTTCCTCCCATCTCACAA (B) PCR of individual CEP290 mutant embryos showing a single band, indicating there is no detectable alternative splicing induced by the mutation. Sequence traces from mutants (C) and heterozygous embryos (D) do not show frameshifts or other indicators of alternative splicing (exon junction indicated by black line) (E) RT-qPCR suggests a slightly lower expression of the mutant allele, but this does not reach statistical significance ($p=0.15$).

Movie S1 *cep290^{sa1383}* mutant cilium movement

Movie S2 WT ear with moving cilia

